Detection and Behavior of Pan Wakes in Saturn's A Ring

LINDA J. HORN

Jet Propulsion Laboratory, 4800 Oak Grove Drive, M/S 183-501, Pasadena, California 91109
E-mail: Linda.J.Horn@jpl.nasa.gov

MARK R. SHOWALTER

Center for Radar Astronomy, Stanford University, Stanford, California 94305

AND

CHRISTOPHER T. RUSSELL

Institute of Geophysics and Planetary Physics, University of California at Los Angeles, Los Angeles, California 90024-1567

Six previously unseen Pan wakes are found interior and exterior to the Encke gap in Saturn's A ring, one in the Voyager 2 photopolarimeter (PPS) stellar occultation data and five in the Voyager 1 radio science (RSS) earth occultation data. Pan orbits at the center of the Encke gap and maintains it. Originally it was hypothesized that a wake would be completely damped by the time it reached a longitude of 360° relative to Pan. However, five of the six newly detected wakes are at longitudes in excess of 360° and are a result of earlier encounters with Pan. The sixth is the first detection of the RSS outer Pan wake. The new PPS inner wake is at a longitude of 389.8°. The new RSS inner wakes are at longitudes of 519.4° ± 1.6° and 879.4° ± 1.6°. The RSS outer wakes are at longitudes of 200.6° ± 1.6°, 560.6° ± 1.6°, and 920.6° ± 1.6°. Because of the time needed for a wake to develop after encountering Pan, the higher order wakes (longitude >360°) can be more prominent than their lower order counterparts which are superimposed at the same location.

The radial dispersion behavior of the Pan wakes are characterized using a Burg autoregressive power spectral algorithm. The wake radial wavelength behavior is compared to a simple model which ignores collisions and self-gravity. The four wakes with longitudes below 360° show an average deviation of 0–3% from the predicted wavelengths, indicative of the strength of collective effects.

The detection of Pan wakes at longitudes greater than 360° demonstrates that wakes persist for much longer than originally hypothesized and may interact with one another. The presence and characteristics of these wakes will provide an important test of kinetic theory models. © 1996 Academic Press, Inc.

1. INTRODUCTION

A small, recently discovered satellite, Pan, appears to be the main cause of the Encke gap in the outer quarter of Saturn's A ring (Showalter 1991). The Encke gap is the second largest gap in the main rings (A, B, and C) and is roughly 325 km wide. Pan maintains the gap, creates wavy edges, generates wakes (quasiperiodic radial structure) in the ring material near the gap, and probably influences a noncircular kinky ringlet near the gap's center. No vertical or horizontal resonances of known satellites fall near the gap edges to assist Pan in maintaining them.

Cuzzi and Scargle (1985) first suggested the existence of a satellite in the Encke gap from Voyager images, which showed wavy gap edges which they hypothesized were produced by the gravitational effects of a small satellite orbiting in the gap. Showalter *et al.* (1986) showed that perturbations by this still unseen satellite could also explain several distinctive gravitational disturbances called wakes in the ring material beyond the gap. A wake is a radial series of slowly varying quasiperiodic maxima and minima in the optical depth that remain stationary in a reference frame which corotates with the satellite. The inner wake leads the satellite in orbital longitude and the outer wake trails it. A stationary observer above the rings would see the wakes change in wavelength and amplitude as Pan moves in its orbit (Showalter *et al.* 1986, Borderies *et al.* 1989, Stewart 1991).

Showalter *et al.* (1986) developed and applied a model to the Voyager 2 photopolarimeter (PPS) stellar occultation data (Esposito *et al.* 1987) and the Voyager 1 radio science (RSS) earth occultation data (Marouf *et al.* 1986) that depicted wake patterns. Both the PPS and RSS occultations produced detailed radial scans of Saturn's main rings. The Voyager 2 PPS observed the star δ Scorpii as it was occulted by Saturn's rings and obtained a ring profile with a raw data radial resolution of roughly 100 m (Lane *et al.*

663

1982). The Voyager 1 RSS experiment also obtained a ring profile, at microwave frequencies of 3.6 and 13 cm, which has been processed to a resolution of several hundred meters or better in the less opaque regions of the A ring (Tyler *et al.* 1981, 1983; Marouf *et al.* 1986).

Showalter *et al.* (1986) inferred the existence and location of a satellite in the Encke gap from the wake signatures including both its orbital radius and its longitude at the Voyager epoch. Showalter (1991) subsequently used this information to detect Pan in 23 Voyager 2 images. To date, Pan has not been reliably detected in any Voyager 1 images. It has an orbital semi-major axis of 133,582.8 ± 0.8 km and is approximately 20 km in diameter if it is composed mainly of water ice (Showalter 1991). Using the Pan discovery images, Showalter calculated that the Voyager 2 PPS inner wake was just 29.8° in longitude away from Pan, the PPS outer wake was at a longitude of 330.2°, and the Voyager 1 RSS inner wake was at a longitude of 159.4° ± 1.6°. These results were very similar to Showalter *et al*'s (1986) original prediction. No RSS outer wake had been detected. Originally it was hypothesized that these wakes would be completely damped by the time they were 360° in longitude away from Pan. Below we show that this supposition is incorrect.

In the section that follows we outline the simple radial wavelength theory for satellite wakes. Then we provide a synopsis of the autoregressive power spectral method developed by Horn (1992) and apply it to the Voyager PPS and RSS profiles.

2. SATELLITE WAKES

The same gravitational forces which produce the wavy Encke gap edges also affect the ring material beyond the gap, producing distinctive signatures coined "wakes" because they are reminiscent of the wake patterns that trail behind a motorboat. In a reference frame that rotates with Pan's orbital velocity, the ring material interior to Pan's orbit slowly moves ahead and the ring material exterior to Pan's orbit slowly drifts behind. Each time a ring particle moves past Pan it experiences a small radial acceleration toward the moonlet, which produces a small "kick" to its orbital eccentricity. Over many orbital periods, the relative phasing of the perturbations on the ring particles produces the wavy gap edges. The successive wave extrema represent the alternating apoapses and periapses of the ring particles on the eccentric orbit. The wavy edge's phasing of pericenters of azimuthal wavelength is $3\pi s$, where s is the radial separation distance between Pan and the ring particles at radius a (Showalter *et al.* 1986). This relationship also holds for ring material further away from the gap edge. As the radial separation distance s increases, the azimuthal wavelength increases also. Since the azimuthal wavelength at two adjacent radial ring locations is slightly
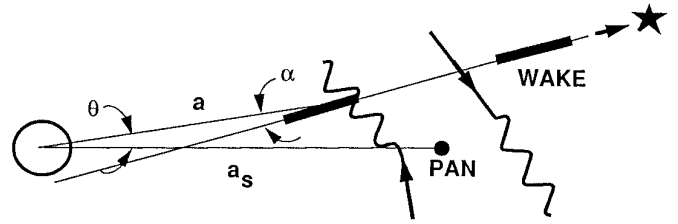

FIG. 1. Satellite wake radial wavelength variation. This schematic depicts the wavy edges and wakes generated by Pan which orbits in the Encke gap. The Encke gap is not to scale with the size and distance from Saturn.

different, over a number of periods the radial oscillations go out of phase, leading to the quasiperiodic optical depth variations known as a wake.

The ring particles subsequently interact via collisions and self-gravity, which can slightly distort the wake pattern and cause it to damp. A wake is not a true "wave" phenomenon however because its propagation does not require any communication between the different wake pieces. Whereas a spiral density wave requires collisions and/or self-gravity to propagate, a wake does not. These collective effects are merely perturbations on a wake pattern, whereas they are a key requirement in order for a wave to exist. Hence, we can reasonably expect to see isolated pieces of a wake on opposite sides of a gap or density wave. Furthermore, the eccentricity "kicks" from successive moon passages add linearly (in a vector sense), so it is possible for different wakes to be superimposed atop of one another. Borderies *et al.* (1989, p. 356) also noted this possibility.

As a wake moves through the rings after an encounter with Pan, its radial wavelength and amplitude slowly change as a function of the longitudinal angle between Pan and the ring particles. Ignoring collective effects such as collisions and self-gravity, and assuming that Pan has negligible orbital eccentricity, the radial wavelength λ_r is given by Showalter *et al.* (1986) as

$$\lambda_r = \frac{3\pi s^2}{a_s |\theta|} \left[1 - \left| \frac{s}{\theta} \right| \tan \alpha \right], \tag{1}$$

where a_s is Pan's semi-major axis, a is the ring particle radius, s is $|a_s - a|$, θ is the longitudinal angle between the ring particles and Pan, and α is the angle between the direction of the occultation scan's footprint and the radial direction in Pan's rotating frame. These parameters are illustrated in Fig. 1. The radial wavelength decreases inversely with θ and increases quadratically with s.

The ring's optical depth variations in a wake are given by Showalter *et al.* (1986) as

$$\tau(r, \theta) = \frac{\tau_o(a)}{1 + 2.24j\mu\eta_o\theta\cos(\eta\theta)\,(a_s/s)^4}, \qquad (2)$$

where τ_o is the unperturbed optical depth, μ is the ratio of the satellite mass to the planetary mass, j is an integer which is -1 for an inner wake and $+1$ for an outer wake, η_o and η are azimuthal wave numbers defined in Showalter *et al.* (1986). As can be seen from Eq. (2), the amplitude increases with increasing longitudinal separation from the satellite. Therefore, if a wake can persist for more than 360°, this "second-order wake" can, in theory, be greater in amplitude than the "first-order" wake on which it is superimposed. However, the wake amplitude cannot grow without bound; eventually particle streamlines are expected to intersect, at which point the wake should damp rapidly. (Streamline crossing would first occur where the denominator in (2) became zero or negative, at which point this simple formula breaks down.) Further work to elucidate the properties and amplitude characteristics of satellite wakes has also been performed by Borderies *et al.* (1989) and Stewart (1991). However, this simple formalism, which neglects the effect of gravitational kicks other than the very first one, is adequate for our initial look at the new data.

Using the radial and longitudinal locations for Pan as determined by Showalter (1991) we can then model the wavelength behavior of the wakes that are detected in the power spectral scans of the Voyager PPS and RSS occultation data.

3. BURG TECHNIQUE

Showalter *et al.* (1986) discovered wakes in the PPS and RSS data by a straightforward "eyeball" search for periodic variations in the rings. For this re-examination of wakes in the Voyager PPS occultation data and RSS occultation data, we use a nonlinear power spectral algorithm called Burg (Burg 1978). A technique was developed by Horn (1992) which uses the Burg algorithm to search for wavelike structure in the Voyager ring data sets. This technique was used to study the wavelength behavior of spiral density waves in the Voyager photopolarimeter (PPS) ring occultation data set (Horn 1992). It was also used to study the characteristic length scales of irregular structure in Saturn's B ring (Horn and Cuzzi 1996). We now apply this same technique to the Voyager PPS and RSS occultation data of Pan's wakes.

The Burg technique is particularly effective for studying quasi-periodic ring structure, such as the Pan wakes, as a function of radial distance. It provides a powerful, objective method for detecting these patterns in the ring data when they may not be obvious to the eye. It has the advantage of not requiring more than one or two cycles to produce meaningful detections. The Burg technique was chosen over the standard Fourier methods because Fourier methods are better suited to large data sets which contain a uniform signal that does not vary with radial distance. In the case of Pan wakes it is more desirable to study short sequences of data.

The algorithm developed by Burg (1978) is a nonlinear autoregressive spectral estimation method for estimating power spectra with high resolution. It works well with a limited sample interval. The Burg algorithm predicts the autocorrelation function beyond the sampled interval of data using the assumption that the estimated power spectrum must be the most random (or have the maximum entropy) of any power spectra which would describe the data. This method solves for poles in the complex z plane. It functions by running both forward and backward error filters over the data. It uses the Levinson (1947) recursion relationship to iteratively calculate a specified number of cofficients in the prediction error filter. This number of coefficients is also referred to as the order of the Burg spectrum. The arithmetic mean of the prediction error variance is successively minimized for each order to ensure stability of the coefficients. These coefficients are then used to calculate a power spectrum. The Burg method is particularly suited for separating closely spaced spectral features in the Burg spectrum.

The Burg autoregressive power spectrum, $S(f)$, is given by

$$S(f) = \frac{2\sigma_a^2}{|1 + \sum_{j=1}^{M} g_i e^{-i2\pi fj}|^2}, \qquad (3)$$

where σ_a is the data variance and g_i are coefficients in the prediction error filter (Ulrych and Bishop 1975). The Burg technique makes use of Eq. (3) to calculate the autoregressive spectral estimate, S. Further details are given in Horn (1992) and Horn and Cuzzi (1996).

4. ANALYSIS METHODS

The process discussed here is used to locate and study the Pan wakes in the PPS and RSS data. First we select a data segment size. This "window" of data is chosen such that large changes in wavelength do not occur over the radial extent of one window. Large wavelength changes within a given window will smear out the power spectral signal and can potentially cause a systematic bias in the frequency estimate. Initially Burg arrays over a variety of window sizes are generated and an optimal window size is chosen. Once the window size is selected then the number of prediction filter coefficients is chosen. These selection processes will be discussed in more detail in the following sections.

For a given window and prediction error filter size, an

array of successive power spectra is generated using the Burg algorithm. The spectra are produced from data segments which overlap by 90% in order to provide more detailed resolution of the wake dispersion.

Finally, we map the power spectral frequency and strength of significant peaks for the Burg spectral array over the radial extent under consideration. Contour plots of the power spectral arrays are generated. In some cases plots of the maximum spectral frequency as a function of distance from Saturn are produced also. We generated and studied Burg spectral arrays for PPS and RSS occultation data on both sides of the Encke gap in search of Pan wakes. Before applying this technique to the wake data we ran some tests on data with known properties.

4.1. Length of Data Segment

Choosing the proper length of the data segments is a key for identifying and studying Pan wakes. If the data window is much smaller than the main wavelength in the data, then the wavelength cannot be correctly identified. If the data window is too large then data nonstationarity within a given data window may potentially cause a systematic bias in the frequency estimate. For this study data windows with radial extents of 15, 22.5, and 30 km were examined. The goal was to assess the magnitude of any bias by essentially halving the data window and comparing corresponding frequency estimates.

An example of this analysis is provided in Fig. 2. Spectra from a portion of the RSS inner wake data are used to provide profiles for data windows of 15, 22.5, and 30 km. This portion of the wake is visible from 133,200 to 133,340 km and ranges in frequency from 0.25 cycles/km (wavelength 4 km) to 0.55 cycles/km (1.8 km). Figure 2 shows the peak spectral frequency from each power spectrum as a function of radial distance. The wake peak frequencies for each window size are comparable. A systematic bias across the wake is not observed over this range of data segments. Using this evaluation of data window of 30 km was selected for this study. This larger window provides a more extended range of resolvable wake frequencies.

4.2. Number of Filter Coefficients

Once the data window has been selected the next step is to choose the number of filter coefficients. If the filter order is too small the spectrum is highly smoothed. Conversely, if the filter order is too large, the resolution of the spectrum is increased but spurious detail is introduced. Ulrych and Ooe (1983) experimentally determined that an order selection of $N/3$ to $N/2$, where N is the number of data points, often produces acceptable results. These assumptions were examined by using a generated sine wave and a data window of 100 data points. Burg spectra of the sine wave were produced using a variety of filter orders

from 10 to 60. A filter order of 30 produced the maximum of value for the spectral peaks. This filter order is close to the $N/3$ value that was experimentally determined by Ulrych and Ooe (1983). Larger or smaller filter orders produced smaller peaks. As the filter size grows to 60, the main peak almost disappears altogether. The results of this analysis are shown in Fig. 3.

The PPS and RSS data themselves were also examined for a variety of filter orders. They produced results similar to those for the sine wave.

4.3. Impact of White Noise on Main Spectra Peaks

Tests were also performed to assess the impact of white noise on the Burg spectrum. A sine wave of known frequency and amplitude was generated. Next, varying amounts of white noise were added to the sine wave data set. The average white noise contribution was varied from zero to 200% of the sine wave amplitude.

Burg spectra were calculated for the various arrays. The data window chosen contained roughly three sine wave cycles. These data were processed in a fashion similar to the ring data. A second-order polynomial fit is first removed before calculating the power spectra. The sine wave data sets are normalized to a standard deviation of 1 after the fit is removed. As expected, as the amount of white noise increases the amplitude of the main peak decreases. When the white noise contribution is 200%, an extreme case, the main peak is barely distinguishable from the noise and is no longer significant. The results of these analyses are shown in Fig. 4. For comparison to the PPS and RSS data, in the vicinity of the Pan wakes a main spectral peak is always readily apparent.

The height of the Burg peak is nonlinear with power. The area under the peak represents the total power rather than the value of the peak amplitude itself. In comparison with spectra generated using the FFT method, the Burg method produces peaks that are more readily apparent when the white noise is in the range of 10–100%. (For additional discussion on comparison of the Burg method to FFT method see Horn and Cuzzi 1996.)

5. RESULTS

Now that Pan has been detected in the Voyager images and its orbital parameters are well determined, we can search the occultation data sets for satellite wakes in regions expected to be influenced by Pan and study their wavelength behavior more carefully. For this paper the Burg data are displayed using a 30-km data window for each data set. The PPS data were first binned by 3 to increase the signal-to-noise ratio and then data windows of 100 points (30 km) were used. The filter order selected for the PPS data was 30. The RSS data window contained 60 points (30 km). A filter order of 20 was selected for the
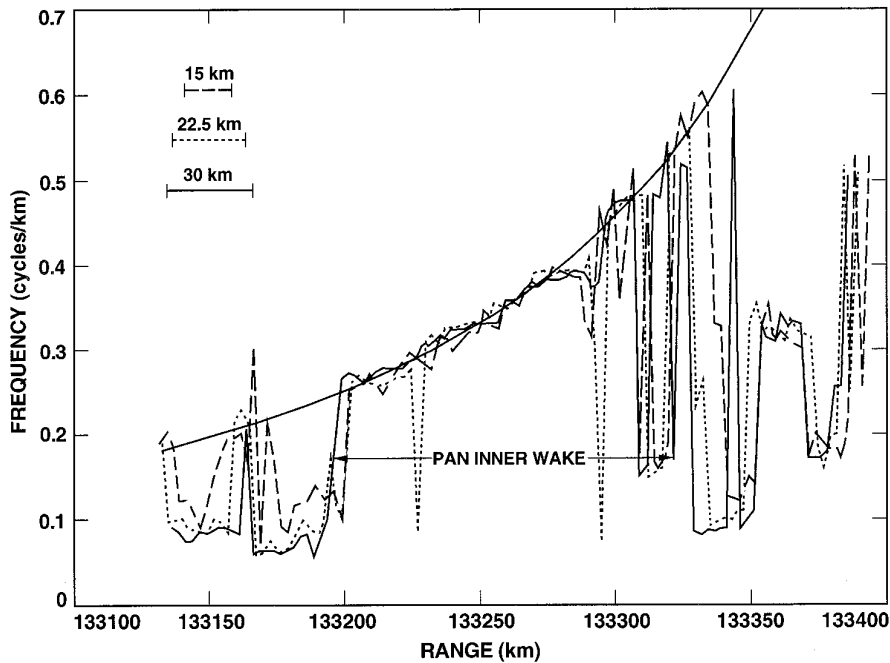
FIG. 2. Peak spectral frequencies for three data window sizes. The peak spectral frequency of each Burg spectrum in the power spectral array is plotted as a function of radial distance for a portion of the RSS inner wake. A best fit to the wake data is overplotted using the reciprocal of Eq. (1). Three data window sizes, 15, 22.5, and 30 km are used to generate the Burg spectra. The wake peak frequencies for each window size are comparable. A systematic bias is not observed in the wake profile as the window size changes by a factor of 2.
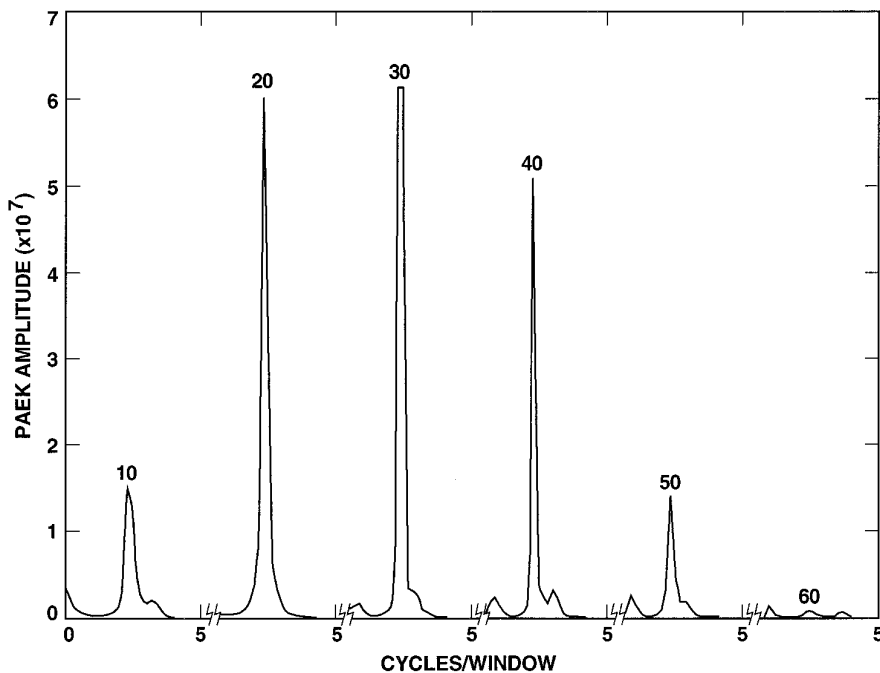

FIG. 3. Sine wave power spectra for prediction error filter orders of 10, 20, 30, 40, 50, and 60. Power spectra are generated for a simple sine wave using a data window of 100 points and a variety of filter orders. The maximum spectral peak occurs for a filter order of 30.
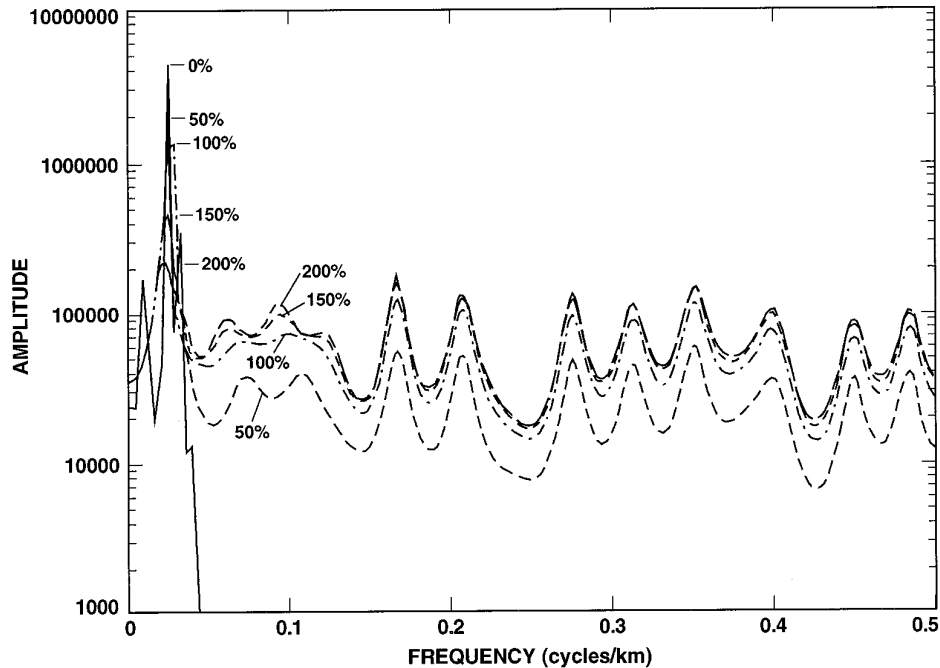
FIG. 4. Burg spectra for sine waves with average white noise contributions of 0 through 200%. After adding the white noise, each data set was normalized to a standard deviation of 1 prior to calculating its Burg spectrum. As the amount of white noise increases the main peak amplitude decreases.

RSS data. The radial scales for these data sets are corrected using the parameters and equations given by Nicholson *et al.* (1990) for the PPS and RSS Saturn ring data. In these spectra we detect evidence for multiple wakes both interior to and exterior to the Encke gap. Our results are summarized in Table I.

5.1. Previously Detected Pan Wakes

Three Pan wakes were detected by Showalter *et al.* (1986). They are the PPS first-order inner and outer wakes

and the RSS first-order inner wake. Using the Burg technique, each of these wakes is easily detected, although in some cases the radial extent over which the wake is observable is substantially greater than that studied by Showalter *et al.* (1986).

5.1.1. PPS First-Order Inner Wake. The PPS first-order inner wake, at a longitude of 29.8°, is the primary wake studied by Showalter *et al.* (1986). It is the most clearly evident Pan wake and falls closer to Pan than any other wake; in fact, it was first noted by Lane *et al.* (1982;

TABLE I
Pan Semi-major Axis* and Collective Effects in Pan Wakes

Data set	Inner/outer wake	Wake long. (deg)	Radial limits of fits (km)	Radial distance[a] from Pan orbit (km)	No. of orbits since Pan encounter	$\Delta\lambda/\lambda_{model}$ (percent)
First-order wakes						
PPS	Inner	29.8°	133250–133425	−336 to −161	22–46	0.1
PPS	Outer	330.2°	133940–134130	354 to 544	149–230	4.2
RSS	Inner	159.4°	133215–133330	−371 to −256	106–154	3.5
RSS	Outer	200.6°	133940–134010	354 to 424	117–140	2.3
Second-order wakes						
PPS	Inner	389.8°	133115–133155	−471 to −431	204–223	3.5
RSS	Inner	519.4	132940–133070	−646 to −516	199–249	5.3
RSS	Outer	560.6	134130–134160	544 to 574	240–254	5.8

[a] Pan semi-major axis is 133,582.8 km. PPS and RSS data were corrected by −2.9 km in order to provide agreement between the fit for the wake at 29.8° and the calculated semi-major axis for Pan.

see their Fig. 9). This wake leads Pan in its orbit. It begins at the Encke gap inner edge at 133,425 km and persists for almost 200 km radially inward to 133,250 km. Figure 5a is the optical depth profile showing the wake. Figure 5b is a contour plot of the Burg spectral features and the wavelength profiles expected from Pan's wakes. Figure 5c is a plot of the peak spectral frequency from each Burg spectrum in the power spectral array as a function of the distance from Saturn. Wake wavelength profiles are overplotted. The theoretical curves for Pan wakes are obtained by plotting the reciprocal of Eq. (1) as a function of radial distance a. This wake ranges in frequency from about 0.2 cycles/km (5 km wavelength) near the gap edge to almost 0.05 cycles/km (20 km wavelength). A second-order wake is also visible near 133,100 km. It is discussed in Section 5.2.2.

Using the simple model defined in Eq. (1) and a longitude of 29.8°, the best fit to this wake, assuming negligible influence from collective effects, produces a semi-major axis for Pan of 133586 ± 1 km. This value is about 3 km larger than the 133582.8 ± 0.8 km value found by Showalter (1991) using the Voyager images. However, when Showalter (1991) reexamined the PPS 29.8° inner wake he found that his best fit to the Pan wake data displayed a constant radial offset of nearly 3 km. This offset is given relative to the absolute radial scale inferred by Nicholson *et al*. (1990). It may indicate that this radial scale currently in use for the PPS Saturn ring data is too large by 2.9 ± 0.8 km, which is within the error of the best radial scale generated to date. Our results, using a different technique on the same data, are consistent with Showalter's interpretation. Adjusting our value by 2.9 km yields an orbital semi-major axis for Pan of 133583.1 km ± 1 km, identical with that of Showalter (1991). The wavelengths measured in this wake appear to be unmodified by collective effects after having encountered Pan a relatively short time ago.

5.1.2. PPS First-Order Outer Wake. The PPS first-order outer wake was originally detected by Showalter *et al*. (1986). This wake is exterior to Pan and trails it, by 330.2° in longitude. The extent of the outer Pan wake detected with the Burg technique is displayed in Fig. 6. This wake is not readily apparent until almost 200 km outside the outer edge of the Encke gap. It is detectable for at least 190 km, from 133,940 to 134,130 km, with a second segment of wake beginning at 134,160 km. Showalter *et al*. initially detected this wake over 170 km, from 133,960 to 134,130 km. The main portion of the wake ranges in frequency from about 0.3 to 0.7 cycles/km (3.3 to 1.4 km wavelength). Figure 6 shows optical depth profiles, Burg contours, and peak spectral frequency profiles for the outer wake and the Prometheus 17:16 density wave. The density wave spectral contour is clearly perturbed, possibly by the Pan outer wake; the wave dispersion pat-

terns in normal density wave spectral contours are more nearly linear (Horn 1992); see Fig. 5.2 for comparison.

The model profile does not match the wake nearly as well as the fit to the inner wake. The wavelength increases by 3%, presupposing a 2.9 km correction in radial scale. Collective effects may be altering the wavelength in this wake pattern, increasing the observed wavelength when compared to the simple theoretical model.

5.1.3. RSS First-Order Inner Wake. The RSS first-order inner wake was first detected by Showalter *et al*. (1986), see also Marouf *et al*. (1986). The orbital parameters from Showalter (1991) produced a longitude of 159.4° ± 1.6° for the inner wake. The longitude of Pan is less certain for the RSS inner wake because Pan was not detected in the Voyager 1 images. Its orbit must be extrapolated from the Voyager 2 images taken almost one year later. The radial scale for this RSS data set was corrected using the Saturn pole and Eq. (6) given in Nicholson *et al*. (1990); the correction to the radial scale was on the order of −9 km.

The inner wake at 159.4° ± 1.6° (see Fig. 4) was not detected by Showalter *et al*. (1986) within the ~100 km closest to the Encke gap inner edge. Showalter *et al*. (1986) initially observed this wake over 115 km, from 133,215 to 133,330 km. The Burg technique detected this wake over 400 km from 132,930 to 133,330 km, spanning both sides of the Pandora 11:10 and Prometheus 15:14 density waves. It ranges in frequency from 0.1 to 0.5 cycles/km (10 to 2 km wavelength) and appears to distort the end of the Pandora 11:10 density wave. Figure 7a is a plot of the RSS optical depth as a function of radial distance from Saturn. Figure 7b is a contour plot which contains only the strongest power spectral peaks and the model wavelength fits for both the first- and second-order Pan wakes. The second-order wake is discussed in Section 5.2.3. The deviation from the model is less than 3% for the first-order wake. Figure 7c compares the wake segment in the region 133,200–133,330 km to the collisionless wake model, using Pan's known radius and longitude. The observed wavelength is large by 3.5%, presumably due to collective effects. This assumes that Showalter (1991) is correct and Nicholson *et al*.'s (1990) radial scale is too high by 2.9 km at the Encke gap.

5.2. Possible New Wakes

Six possible new wake-like patterns have been identified in the PPS and RSS data sets. They include the RSS first-order outer wake, three second-order wakes, one in the PPS data and two in the RSS data, and possibly two third-order wakes in the RSS data.

5.2.1. RSS First-Order Outer Wake.

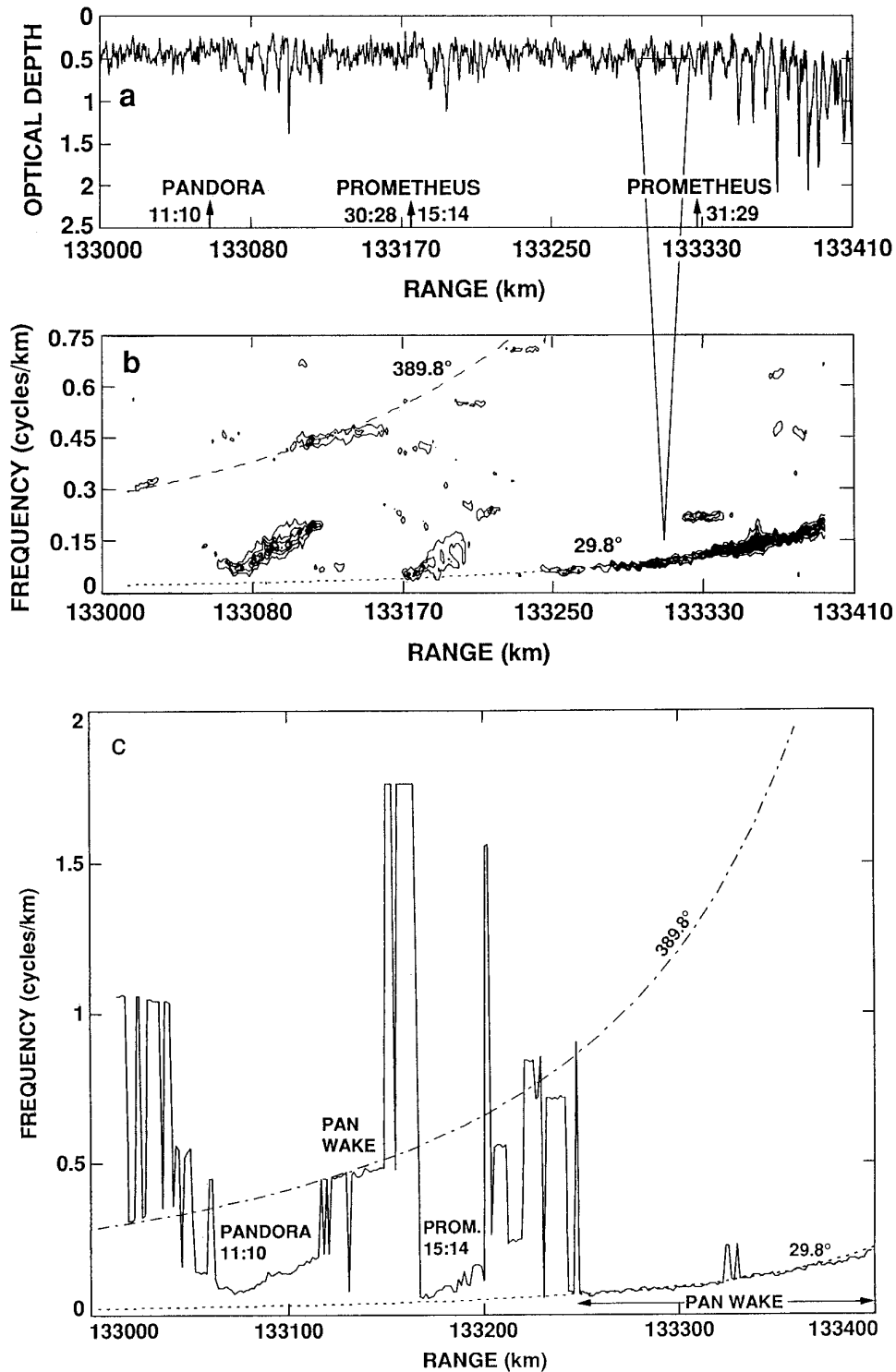The RSS first-order outer wake was not detected by Showalter *et al*. (1986). Given the leading/trailing symmetry

FIG. 5. Two Pan inner wakes in PPS data. (a) A PPS optical depth profile of the region interior to the Encke gap is displayed. The Encke gap begins just off the right-hand side of the plot. The wavy structure on the right side of the plot is the Pan 29.8° wake. Lindblad resonance locations are indicated by arrows and two of the associated density waves are easily visible, the Pandora 11:10 and Prometheus 15:14. The 30-km width of the triangle is the width of the data window used in examining the data. (b) Burg contour and models of Pan 29.8° and 389.8° wakes. Power spectral peaks with the largest values are contoured. The dotted line represents the model of the Pan 29.8° wake and dashed line represents the model of the Pan 389.8° wake. (c) The peak spectral frequency of each Burg spectrum in the power spectral array is plotted as a function of radial distance for the region containing the PPS inner wakes. Model fits to the wake data are overplotted using the reciprocal of Eq. (1) and the appropriate Pan longitudes. The first- and second-order wakes, Pandora 11:10 density wave, and Prometheus 15:14 density wave are labeled.
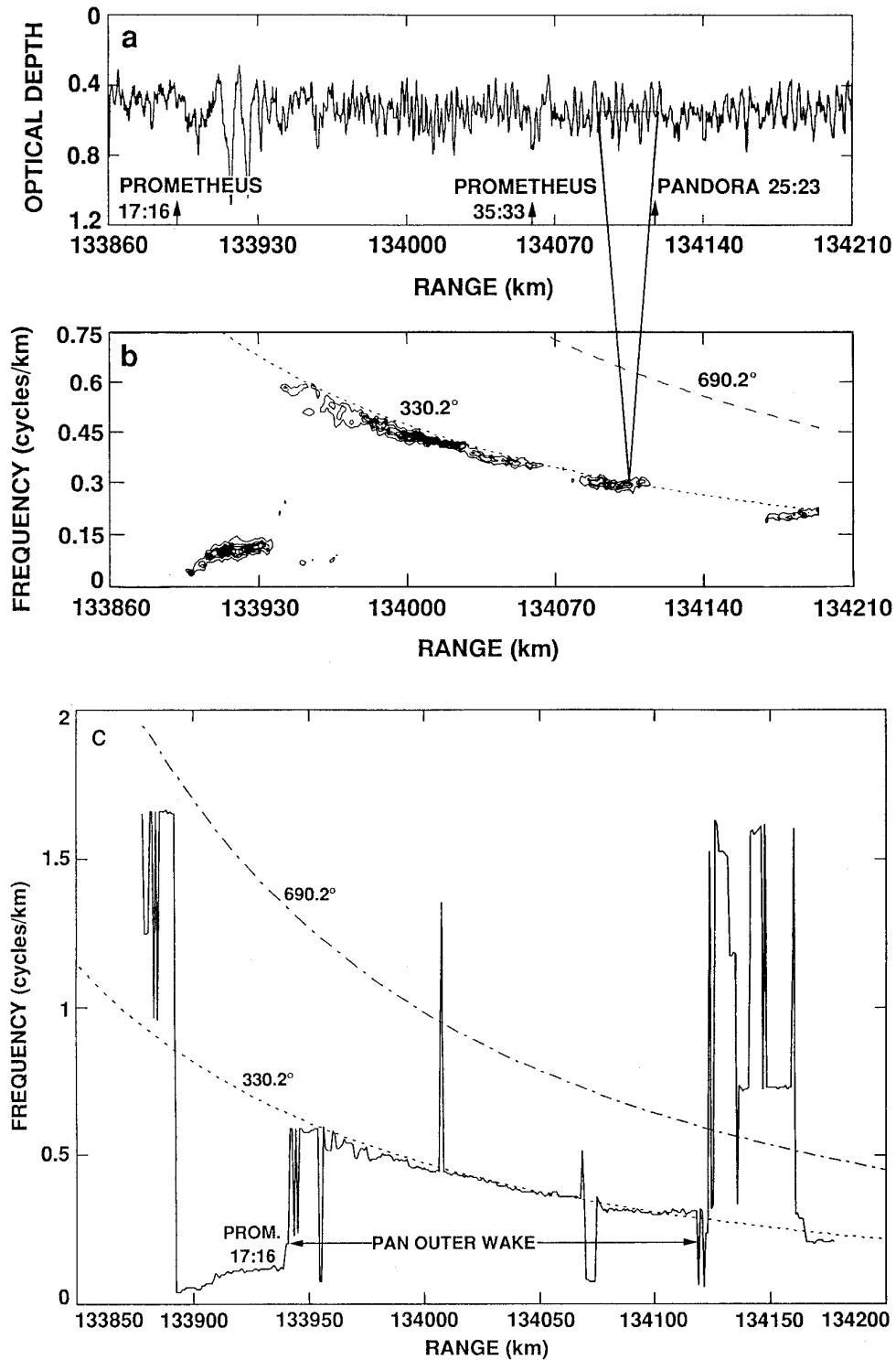
FIG. 6. Pan outer wake in PPS data. (a) A PPS optical depth profile of the region exterior to the Encke gap is displayed. The Encke gap ends about 135 km before the beginning of the left-hand side of the plot. Lindblad resonance locations are indicated by arrows and one of the associated density waves is easily visible, the Prometheus 17:16. The 30-km width of the triangle is the width of the data window used in examining the data. (b) Burg contour and model of Pan 330.2° wake. Power spectral peaks with the largest values are contoured. The dotted line represents the model of the Pan 330.2° wake and dashed line represents the model of the Pan 690.2° wake. (c) The peak spectral frequency of each Burg spectrum in the power spectral array is plotted as a function of radial distance for the region containing the PPS outer wake. Model fits to the wake data are overplotted using the reciprocal of Eq. (1) and the appropriate Pan longitudes. The first-order outer wake and Prometheus 17:16 density wave are labeled.
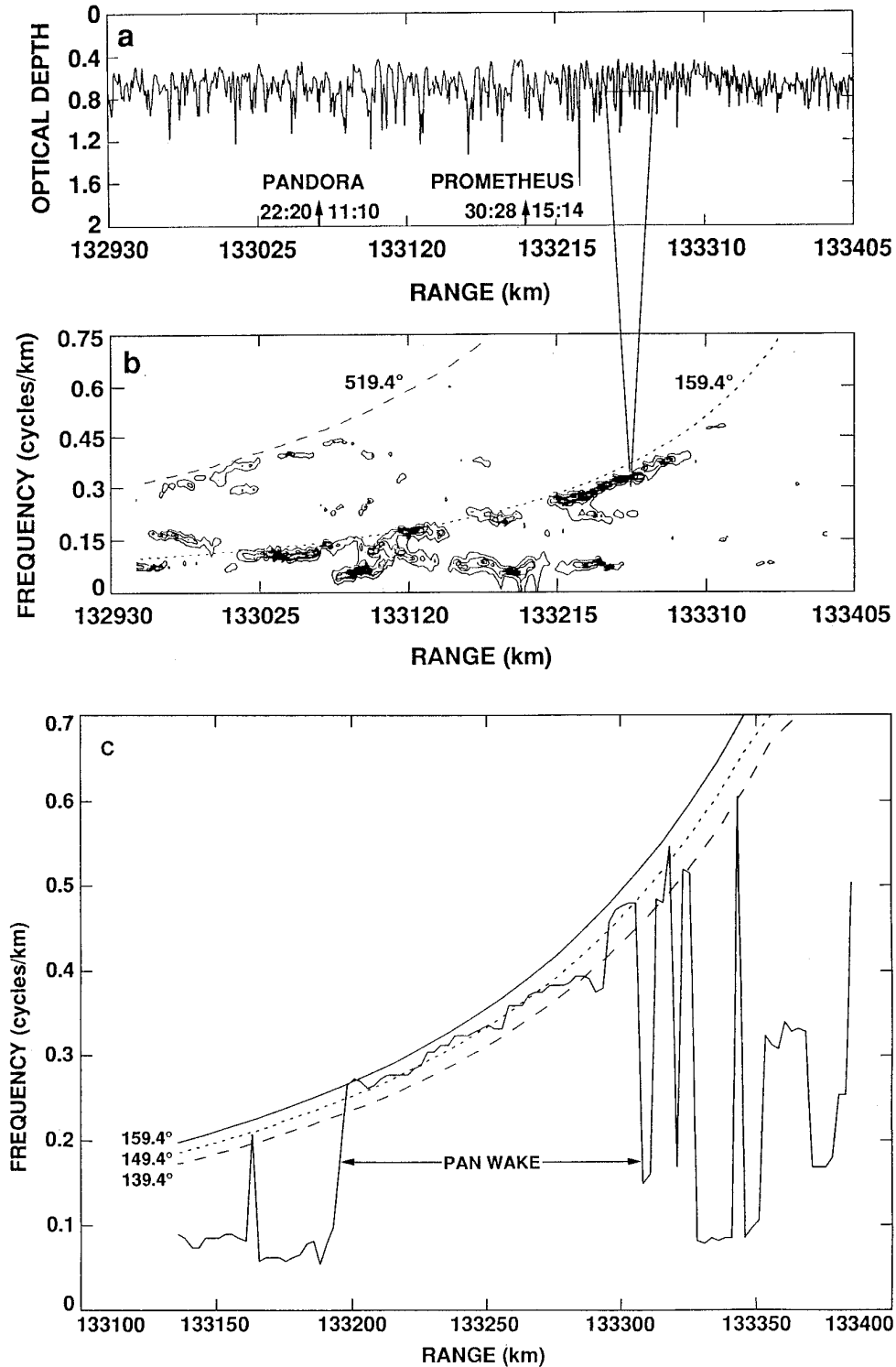
FIG. 7. Pan inner wakes in RSS data. (a) An RSS optical depth profile of the region interior to the Encke gap is displayed. The Encke gap begins just off the right-hand side of the plot. Lindblad resonance locations are indicated by arrows and two of the associated density waves are visible, the Pandora 11:10 and Prometheur 15:14. The 30-km width of the triangle is the width of the data window used in examining the data. (b) Burg contour and models of Pan 159.4° and 519.4° wakes. Power spectral peaks with the largest values are contoured. The dotted line represents the model of the Pan 159.4° wake and the dotted line represents the model of the Pan 519.4° wake. Collective effects produce noticeable offsets from the simple model. (c). The peak spectral frequency of each Burg spectrum in the power spectral array is plotted as a function of radial distance for the region containing the RSS first-order inner wake. Model fits to the wake data are overplotted using the reciprocal of Eq. (1) and longitudes separated by 10°.

for the Pan wakes, the outer wake should be found near a longitude of 200.6° ± 1.6°. We searched the RSS data exterior to the Encke gap and discovered a feature in the Burg contour that looked remarkably like an outer wake (see Fig. 8). It displays a decrease in frequency with increasing radial distance from Saturn, unlike density waves which all exhibit the opposite trend. This feature is easily detected over 70 km, from 133,940 to 134,010 km. Its frequency ranges from 0.15 to 0.3 cycles/km (6.7 to 3.3 km wavelength).

We tested this feature to see if it is indeed a wake by comparing it to a wake frequency profile generated using Showalter's semi-major axis for Pan and a longitude of 200.6°. The distinct portion of the pattern fell very close to the model, deviating by less than 3%. We identify this pattern as the RSS 200.6° outer wake. Figure 8a is a plot of the RSS optical depth as a function of distance from Saturn. Figure 8b is a contour plot of the strongest spectral peaks. Model wavelengths for Pan's first and second-order wakes are overplotted. The second-order wake is discussed in Section 5.3.2. Figure 8c compares the first-order wake segment to the collisionless wake model, using Pan's known radius and longitude. The observed wavelength is larger than the model wavelength by 2.3%, presumably due to collective effects.

5.2.2. PPS Second-Order Inner Wake. Radially inward from the prominent PPS inner wake we find evidence for another wakelike pattern, seen in Fig. 5 between 133,115 and 133,155 km. It lies between the Pandora 11:10 and Prometheus 15:14 spiral density wave signatures and ranges in frequency from 0.4 to 0.5 cycles/km (2.5 to 2.0 km wavelength). This pattern is unlike typical density waves which begin at much lower frequencies (see density wave patterns in Fig. 5).

At first we considered several possible explanations for this pattern. We speculated that it might be a disruption in the Pandora 11:10 density wave perhaps caused by a sudden, unexplained change in surface mass density. It might also be the wake of a previously undetected satellite in the Encke gap or perhaps a second-order wake caused by Pan.

The density wave disruption hypothesis is unlikely because the surface mass densities calculated for the Pandora 11:10 and Prometheus 15:14 density waves are essentially within the error bars of one another (Holberg *et al.* 1982, Nicholson *et al.* 1990, Rosen *et al.* 1991, Horn 1992). For this hypothesis to be true, two surface mass density disruptions are needed, one to cause the shift in the Pandora 11:10 density wave and the second to cause a shift back to the original surface mass density just before the Prometheus 15:14 density wave begins. Two shifts, with one exactly canceling the other, seem very improbable. Furthermore, no comparable change in the local optical depth is observed.

Assuming that the pattern represents a wake, we performed an orbital fit over a range of radii that spanned the entire Encke gap and over a full range of longitudes. No minimum, or best fit, occurred in 360° of longitude, implying that the pattern is not a first-order wake of an additional satellite in the Encke gap.

Next, the possibility of a higher order Pan wake was examined. The first higher order PPS wake will be a full 360° way from the prominent wake, at a longitude of 389.8° with respect to Pan. As can be seen in Fig. 5, a 389.6° model profile fits the data quite well. Another small piece of this wake is visible over 100 km closer to Saturn (~133,010 km) with a frequency of about 0.3 cycles/km (3.3 km wavelength). We identify both segments as part of a second-order Pan wake, detected between 133,010 and 133,155 km.

This wake, the density waves, and the wavelength fit using the reciprocal of Eq. (1) as a function of *a* and Pan's longitude values from Showalter (1991) are displayed in Fig. 5. This set of contours is slightly further away from the model profile than those for the RSS 159.4° wake, corresponding to an increase in wavelength of 3.5%.

5.2.3. RSS Second- and Third-Order Inner and Outer Wakes. A second-order wake-like pattern is just visible in the RSS inner wake data essentially superimposed on a portion of the RSS first-order inner wake (Fig. 7). It ranges from roughly 132,940 to 133,070 km and spans a range of frequencies that are higher than a typical density wave. It ranges in frequency from 0.3 to 0.45 cycles/km (3.3 to 2.2 km wavelength). It is visible in Fig. 7 as a faint set of contours just below the dashed line which indicates the frequency dispersion from the simple model for a wake at a longitude of 519.4°. This set of contours is slightly further away from the model profile than those for the RSS 159.4° wake, corresponding to an increase in wavelength of about 5.3%. This is indicative of an even stronger influence from collective effects. This second-order wake has existed for a longer time than the first-order wake and collective effects have had a longer time to alter the wavelength of the higher order wake.

Another second-order wake is also just visible in the RSS outer wake data in Fig. 8. It is visible in Fig. 8 as a faint set of contours just below the dashed line which indicates the frequency dispersion using the model for a wake at a longitude of 560.4°. This set of contours is slightly further away from the model profile, corresponding to an increase in wavelength of about 5.8%. This is indicative once again of the strengthening of collective effects.

Figure 9 shows Burg spectral results that have been contoured to reveal even small spectral peaks in an effort to search for possible third-order Pan wakes. Three model profiles are overplotted in each case. Figure 9a is a contour of the region containing the Pan inner wakes in the RSS data. The two inner wakes discussed previously (159.4° and 519.4°) are visible in this data set. Pieces of a possible third-
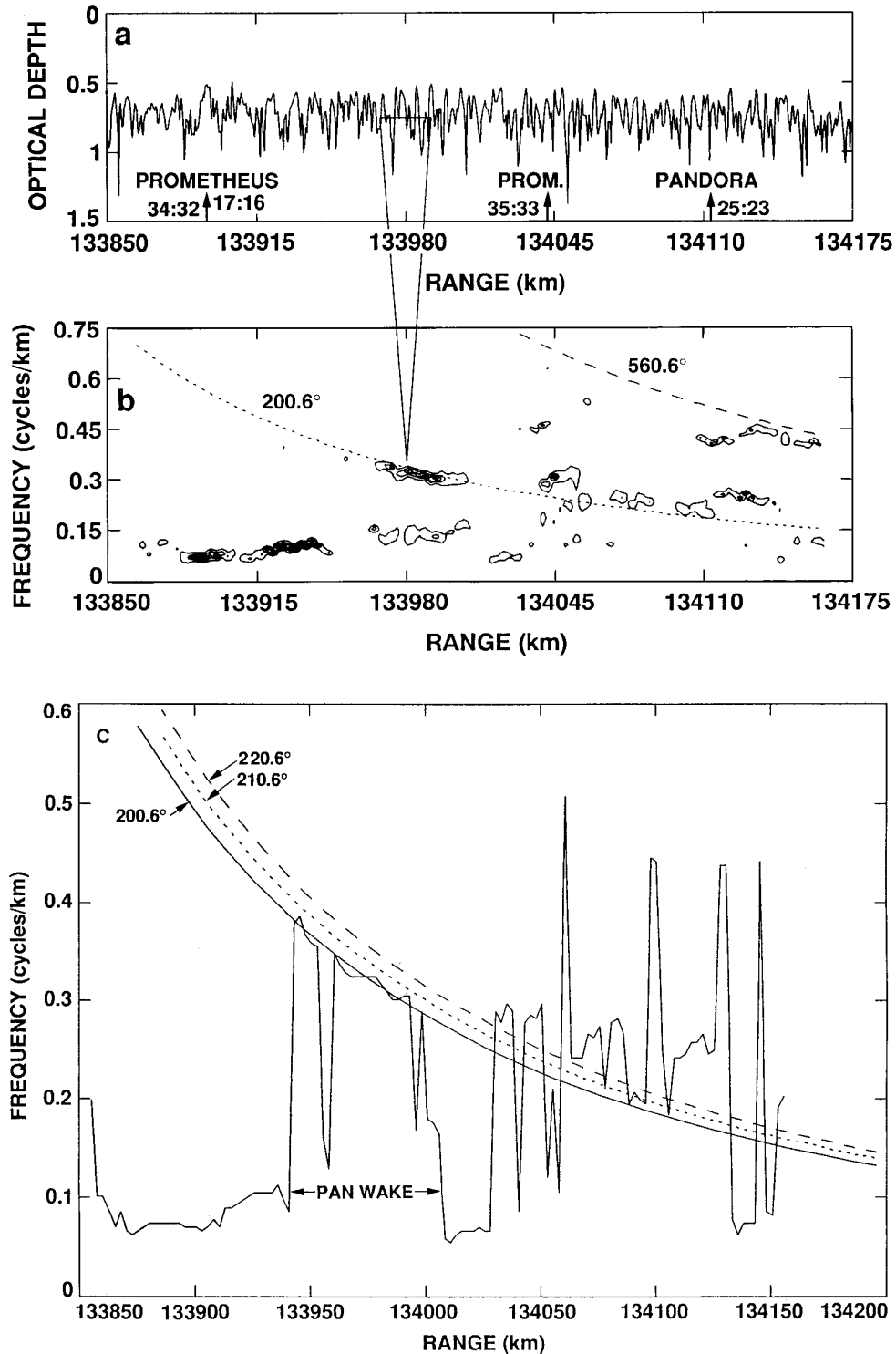
FIG. 8. Pan outer wakes in RSS data. (a) An RSS optical depth profile of the region exterior to the Encke gap is displayed. The Encke gap ends about 125 km before the beginning of the left-hand side of the plot. Lindblad resonance locations are indicated by arrows and one of the associated density waves is visible, the Prometheus 17:16. The 30-km width of the triangle is the width of the data window used in examining the data. (b) Burg contour and models of Pan 200.4° and 560.4° wakes. Power spectral peaks with the largest values are contoured. The dotted line represents the model of the 200.6° Pan wake and the dashed line represents the model of the 560.4° wake. Collective effects produce offsets between the model and the data. (c) The peak spectral frequency of each Burg spectrum in the power spectral array is plotted as a function of radial distance for the region containing the RSS first-order outer wake. Model fits to the wake data are overplotted using the reciprocal of Eq. (1) and longitudes separated by 10°.
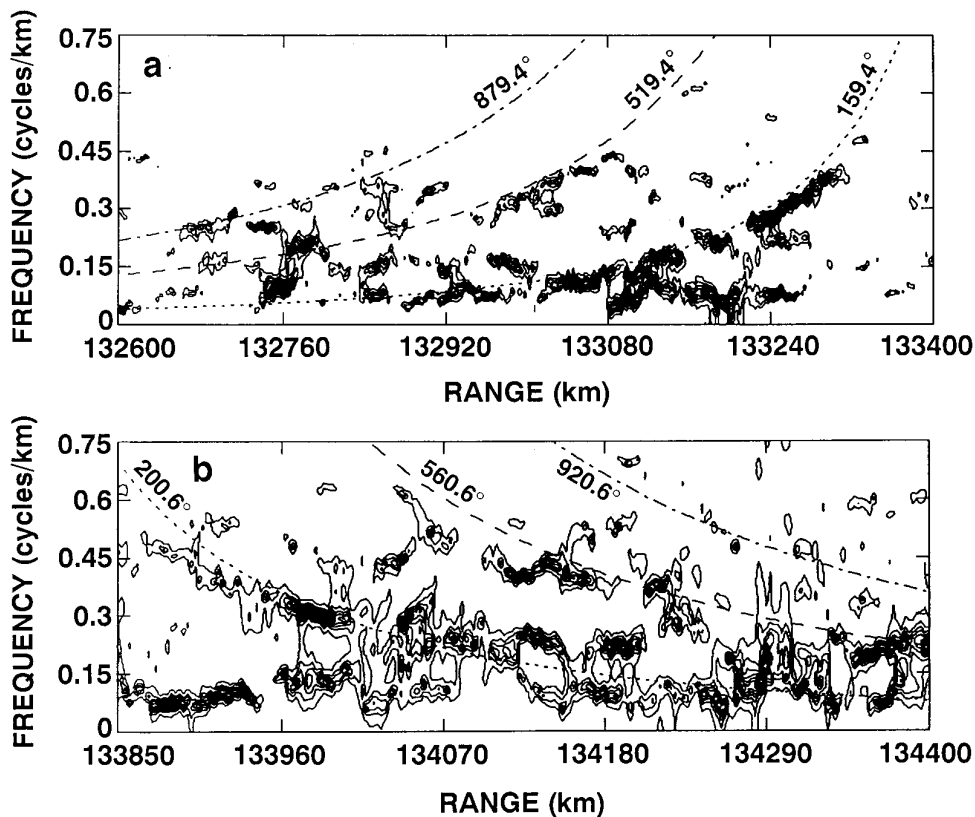
FIG. 9. RSS Burg contours of regions containing Pan inner and outer wakes. (b) Burg contour models of Pan 200.4°, 560.4°, and possible 920.4° wakes. The Burg spectral array has been contoured to reveal even small spectral peaks in order to search for third-order Pan wakes. A possible wake at 920.4° has been identified. (a) Burg contour and models of Pan 159.6°, 519.6°, and possible 879.6° wakes. The Burg spectral array has been contoured to reveal even small spectral peaks in order to search for third-order wakes. A wake may just barely be detectable at 879.6°.

order wake at 879.4° are just visible on the left side of the contour. This contour covers a more extended region or the RSS data than displayed previously. It is also interesting to note the large radial extent of wake propagation for the 159.4° wake in this profile (running from at least 132,900 to 133,320 km).

Figure 9b is a contour of the regions containing the Pan outer wakes in the RSS data. The two outer wakes discussed previously (200.6° and 560.6°) are also visible in this contour. It is interesting to note the large radial extent of the Prometheus 17:16 density wave (extending from 133,850 to at least 134,100 km and, using a linear extrapolation, perhaps as far as 134,200 km). A hint of a possible third-order wake at 920.6° is just visible.

6. CONCLUSIONS AND FUTURE WORK

We confirm the conclusion of Showalter *et al.* (1986) that Pan is the dominant mass in the Encke gap. Of the numerous wake patterns detected near the gap, all of them can be directly attributed to Pan. Any other nearby

moon comparable in mass to Pan would have definitely turned up in this analysis.

Collective effects play a slight but noticeable role in modifying the waves. In all of the patterns observed (except the 29.8° wake in the inner PPS data), the wavelength increases relative to the collisionless model, typically by a few percent. This seems to be consistent with the model of collective effects by Showalter *et al.* (1986, Appendix A), who showed that self-gravity initially dominates over collisions in a wake pattern, and that it tends to increase the local wavelength. However, collisions eventually come to dominate when the wake streamlines approach the point of crossing, and these tend to decrease the wavelength. Since the wakes detected in this study are rather low in amplitude, it is perhaps not surprising that their wavelengths are increased. By contrast, Borderies *et al.* (1989) did not allow for wavelength variations in their analysis.

The discovery of Pan wakes at longitudes greater than 360° indicates that wakes can persist from one Pan encounter to the next. It follows that they are not the short time

scale phenomena originally envisioned; at least at greater radial distances from the moon, the effects on one gravitational encounter persist to the next and the new wake may contain a memory of the previous encounter. The current theories of wakes and of the shepherding process assume that the ring particles begin each moon encounter unperturbed. This assumption is now challenged by the observations, suggesting that further dynamic modeling will be needed.

In addition to revealing how a moonlet wake evolves, this paper has also demonstrated the remarkable capabilities of the Burg method for identifying subtle, quasiperiodic patterns in ring occultation data. In the future, we will search more widely through the PPS and RSS data sets to identify other waves and wakes, in the hopes that this will tell us more about the interactions between rings and small moonlets in Saturn's ring system.

ACKNOWLEDGMENTS

REFERENCES

BORDERIES, N., P. GOLDREICH, AND S. TREMAINE 1989. The formation of sharp edges in planetary rings. *Icarus* **80,** 344–360.

BURG, J. P. 1978. A new analysis for time series data. In *Modern Spectrum Analysis* (D. G. Childers, Ed.), pp. 42–48. Wiley–Interscience, New York. (Presented at NATO Advanced Study Institute of Signal Processing with Emphasis on Underwater Acoustics, August, 1968.)

CUZZI, J. N., AND J. D. SCARGLE 1985. Wavy edges suggest moonlet in Encke's gap. *Astrophys. J.* **292,** 276–290.

ESPOSITO, L. W., C. C. HARRIS, AND K. E. SIMMONS 1987. Features in Saturn's rings. *Astron. J. Supp. Ser.* **63,** 749–770.

HOLBERG, J. B., W. FORESTER, AND J. J. LISSAUER 1982. Identification of resonance features within the rings of Saturn. *Nature* **297,** 115–120.

HORN, L. J. 1992. *Wave Structure in Planetary Rings.* Ph.D. thesis, University of California at Los Angeles.

HORN, L. J., AND J. N. CUZZI 1996. Characteristic wavelengths of irregular structure in Saturn's B ring. *Icarus* **119,** 285–310.

LANE, A. L., C. W. HORD, R. A. WEST, L. W. ESPOSITO, D. L. COFFEEN, M. SATO, K. E. SIMMONS, R. B. POMPHREY, AND R. B. MORRIS 1982. Photopolarimetry from Voyager 2: Preliminary results on Saturn, Titan, and the rings. *Science* **215,** 537–543.

LEVINSON, N. 1947. The Wiener RMS (root mean square) error criterion in filter design and prediction. *J. Math. Phys.* **25,** 261–278.

MAROUF, E. A., G. L. TYLER, AND P. A. ROSEN 1986. Profiling Saturn's rings by radio occultation. *Icarus* **68,** 120–166.

NICHOLSON, P. D., M. L. COOKE, AND E. PELTON 1990. An absolute radius scale for Saturn's rings. *Astron. J.,* **100,** 1339–1362.

ROSEN, P. A., G. L. TYLER, E. A. MAROUF, AND J. J. LISSAUER 1991. Resonance structures in Saturn's rings probed by radio occultation. II. Results and interpretation. *Icarus* **93,** 25–44.

SHOWALTER, M. R. 1991. Visual detection of 1981S13, Saturn's eighteenth satellite, and its role in the Encke gap. *Nature* **351,** 709–713.

SHOWALTER, M. R., J. N. CUZZI, E. A. MAROUF, AND L. W. ESPOSITO 1986. Satellite "wakes" and the orbit of the Encke gap moonlet. *Icarus* **66,** 297–323.

STEWART, G. R. 1991. Nonlinear satellite wakes in planetary rings. *Icarus* **94,** 436–450.

TYLER, G. L., E. A. MAROUF, R. A. SIMPSON, H. A. ZEBKER, AND V. R. ESHLEMAN 1983. The microwave opacity of Saturn's rings at wavelengths of 3.6 and 13 cm from Voyager 1 radio occultation. *Icarus* **54,** 160–188.

TYLER, G. L., V. R. ESHLEMAN, J. D. ANDERSON, G. S. LEVY, G. F. LINDAL, G. E. WOOD, AND T. A. CROFT 1981. Radio science investigations of the Saturn system with Voyager 1: Preliminary results. *Science* **212,** 201–206.

ULRYCH, T. J., AND T. N. BISHOP 1975. Maximum entropy spectral analysis and autoregressive decomposition. *Rev. Geophys. Space Phys.* **13**(1), 183–200.

ULRYCH, T. J., AND M. OOE 1983. Autoregressive and mixed ARMA models and spectra. In *Nonlinear Methods of Spectral Analysis* (S. Haykin, Ed.), 2nd ed., Chap. 3. Spring-Verlag, New York.